International Journal of Heat and Mass Transfer 52 (2009) 1005–1011

Contents lists available at ScienceDirect

International Journal of Heat and Mass Transfer

journal homepage: www.elsevier.com/locate/ijhmt

Transient radiative heating characteristics of slabs in a walking beam type reheating furnace

Sang Heon Han [a,*], Seung Wook Baek [a], Man Young Kim [b]

[a] Department of Aerospace, Korea Advanced Institute of Science and Technology, 373-1 Guseong-dong, Yuseong-gu Daejeon 305-701, Republic of Korea
[b] School of Mechanical and Aerospace Systems Engineering, Chonbuk National University, 664-14 Duckjin-dong, Duckjin-gu, Jeonju, Chonbuk 561-756, Republic of Korea

ARTICLE INFO

Article history:
Received 29 March 2007
Received in revised form 14 March 2008
Available online 22 September 2008

Keywords:
Reheating furnace
Radiative slab heating
Residence time

ABSTRACT

Transient radiative heating characteristics of slabs in a walking beam type reheating furnace is predicted by the finite-volume method (FVM) for radiation. The FVM can calculate the radiative intensity absorbed and emitted by hot gas as well as emitted by the wall with curvilinear geometry. The non-gray weighted sum of gray gas model (WSGGM) which is more realistic than the gray gas model is used for better accurate prediction of gas radiation. The block-off procedure is applied to the treatment of the slabs inside which intensity has no meaning. Entire domain is divided into eight sub-zones to specify temperature distribution, and each sub-zone has different temperatures and the same species composition. Temperature field of a slab is acquired by solving the transient 3D heat conduction equation. Incident radiation flux into a slab is used for the boundary condition of the heat conduction equation governing the slab temperature. The movement of the slabs is taken into account and calculation is performed during the residence time of a slab in the furnace. The slab heating characteristics is also investigated for the various slab residence times. Main interest of this study is the transient variation of the average temperature and temperature non-uniformity of the slabs.

1. Introduction

One of major concerns regarding a reheating furnace is heating characteristics of slabs. There are two requirements for a slab to satisfy before its exit to the rolling mill. While the temperature of a slab should be elevated up to intended temperature, the temperature gradient inside the slab should remain below 50 K/m before its exit. The second largest energy is consumed to reheat slabs before rolling process in hot strip mill while the largest energy is consumed in the process of melting ore. A great deal of attention is thus needed to reduce some parts of unnecessary energy consumption to increase the performance of a furnace. Since a decrease in energy consumption can directly reduce the generation of carbon dioxide, the performance of a reheating furnace is very important. In view of performance, the shorter residence time of slabs is highly desirable while maintaining uniform temperature inside slabs.

It is well known that radiative heat transfer is a major heat transfer mode to heat up slabs inside a reheating furnace. Over 90% heat transfer is via radiation [1,2]. Radiation emitted by hot gas and hot furnace walls reaches to slabs and is then absorbed into slabs. The absorbed radiation is converted into heat and the heat further penetrates into slabs by means of conduction. Importance of radiative heat transfer in heating slabs is well reflected by the previous study of a reheating furnace. Li et al. [3] calculated radiative heating of a slab in a pusher type furnace chamber using zone method. They used simplified furnace chamber and calculated the slab temperature in two dimension. Anton et al. [4] predicted the influence of the space between billets on the productivity of a walking beam type furnace by using Monte Carlo method.

The present work is to simulate the transient radiative heating characteristics of slabs in a POSCO furnace. The finite-volume method (FVM) is used for treating radiation emitted by the walls and gas. The weighted sum of gray gas model (WSGGM) is adopted to take into account the hot gas radiation effect. And the effect of variation of residence time is pursued in this research. The FVM for radiation which is the same family of the DOM [5–7] was derived by Chui and Chai [8–10] to study thermal radiation in a irregular or curvilinear grid. It has been successfully applied to a problem of two-dimensional curvilinear cavity. Kim and Baek [11] also applied it for analyzing combined conduction, convection and radiation in a gradually expanding channel. They also extended the method to 3D geometry [12]. The FVM can be easily applied to body-fitted coordinates and unstructured mesh [13], since the conservation constraint resulting from integrating the RTE over a control volume and a control angle is satisfied. In this method, the inflow and outflow of radiant energy across control volume faces are balanced with attenuation and augmentation of

* Corresponding author. Tel.: +82 42 869 3754; fax: +82 42 869 3710.
E-mail address: freezia@kaist.ac.kr (S.H. Han).

0017-9310/$ - see front matter © 2008 Elsevier Ltd. All rights reserved.
doi:10.1016/j.ijheatmasstransfer.2008.07.030

Nomenclature

C	specific heat capacity of slab
D_{ci}^{m}	directional weights
$f_{\varepsilon,k}$	weighting factor used in WSGGM
I	actual radiation intensity (W/(m^2 sr))
I_b	blackbody radiation intensity, $=\sigma T^4/\pi$ (W/(m^2 sr))
M	total number of radiation direction
$\vec{n}_i$	unit normal vector at i surface
q_w^R	wall radiation flux (W/m^2)
$\vec{r}$	position vector (m)
$\vec{s}$	unit direction vector
T	temperature (K)
t	time (s)
x, y, z	axes of Cartesian coordinate (m)

Greek symbols

β_0	extinction coefficient, $=\kappa_a+\sigma_s$ (m^{-1})
ΔA_i, ΔV	surface area and volume of the control volume, respectively
$\Delta\Omega^m$	discrete control angle (sr)
ε_w	wall emissivity
ρ	density of slab (kg/m^3)
θ	polar angle measured from the z-axis (rad)
κ_a	absorption coefficient (m^{-1})
λ	thermal conductivity of a slab (W/(m K))
σ	Stefan–Boltzmann constant, $=5.67\times10^{-8}$ (W/(m^2 K^4))
σ_s	scattering coefficient (m^{-1})
Φ	phase function of scattering
ϕ	azimuthal angle measured from the x-axis (rad)
Ψ	scattering angle between $\vec{s}'$ and $\vec{s}$
ω_0	scattering albedo, $=\sigma_s/\beta_0$

Superscripts

m, n	radiation direction
o	previous time step
old	previous iteration step
R	radiation

Subscripts

E, W, N, S, T, B	east, west, north, south, top and bottom neighbors of P
e, w, n, s, t, b	east, west, north, south, top and bottom control volume faces
k	kth gray gas
P	nodal point in which intensities are located
slab	slab
w	wall

radiant energy within a control volume and a control angle. Total solid angle, 4π, is discretized into a finite number of discrete solid (control) angle in any convenient manner.

2. Mathematical formulation

2.1. Treatment of slabs

Temperature field of a slab is governed by the following transient heat conduction equation:

$$\rho C\frac{\partial T}{\partial t}=\frac{\partial}{\partial x}\left(\lambda\frac{\partial T}{\partial x}\right)+\frac{\partial}{\partial y}\left(\lambda\frac{\partial T}{\partial y}\right)+\frac{\partial}{\partial z}\left(\lambda\frac{\partial T}{\partial z}\right) \tag{1}$$

Here ρ, C, λ are mass density, specific heat capacity, and thermal conductivity of a slab, respectively. The incident radiation flux to the slab is used for the boundary condition of Eq. (1):

$$q_{slab}^{R}=\int_{\Omega=4\pi} I(\vec{r}_w,\vec{s})(\vec{s}\cdot\vec{n}_w)\mathrm{d}\Omega \tag{2}$$

Integration of Eq. (1) on a cell control volume gives a discretized equation which relates temperature of the cell with the temperatures of the neighboring cells:

$$a_P T_P=a_E T_E+a_W T_W+a_N T_N+a_S T_S+a_T T_T+a_B T_B+S_P \tag{3a}$$

where

$$a_I=\frac{\lambda_i A_i}{(\delta x)_i},\quad I=\mathrm{E,W,N,S,T,B},\quad i=\mathrm{e,w,n,s,t,b} \tag{3b}$$

$$a_P=\sum_{I=\mathrm{E,W,N,S,T,B}} a_I+\frac{\rho C\Delta V}{\Delta t} \tag{3c}$$

$$S_P=\frac{\rho C\Delta V}{\Delta t}T_P^{o} \tag{3d}$$

In the above equation, subscript I denotes a neighboring cell while i denotes the interfacial surface between the current cell and a neighboring cell. $(\delta x)_i$ is the distance between the current cell and a neighboring cell.

It is assumed that slabs move quick and quiet. On this assumption, it takes no time for slabs to move next positions. So movement of a slab is processed by just transferring temperature data of previous location to those of next location during calculation.

2.2. Finite-volume method for radiation

The radiation intensity for gray medium at any position, $\vec{r}$, along a path, $\vec{s}$ through an absorbing, emitting and scattering medium is given by

$$\frac{1}{\beta_0}\frac{\mathrm{d}I(\vec{r},\vec{s})}{\mathrm{d}s}=-I(\vec{r},\vec{s})+(1-\omega_0)I_b(\vec{r})+\frac{\omega_0}{4\pi}\times\int_{\Omega'=4\pi} I(\vec{r},\vec{s}')\Phi(\vec{s}'\to\vec{s})\mathrm{d}\Omega' \tag{4}$$

where $\beta_0=\kappa_a+\sigma_s$ is the extinction coefficient, and $\omega_0=\sigma_s/\beta_0$ is the scattering albedo. $\Phi(\vec{s}'\to\vec{s})$ is the scattering phase function for radiation from incoming direction $\vec{s}'$ to scattered direction $\vec{s}$. This equation, if temperature of the medium, $I_b(\vec{r})$ and boundary conditions for intensity are given, provides a distribution of the radiation intensity in medium. The boundary condition for a diffusely emitting and reflecting wall can be denoted by

$$I(\vec{r}_w,\vec{s})=\varepsilon_w I_b(\vec{r}_w)+\frac{1-\varepsilon_w}{\pi}\int_{\vec{s}'\cdot\vec{n}_w<0} I(\vec{r}_w,\vec{s}')|\vec{s}'\cdot\vec{n}_w|\mathrm{d}\Omega' \tag{5}$$

where ε_w is the wall emissivity and $\vec{n}_w$ is the unit normal vector at the wall. The above equation illustrates that the leaving intensity from the wall is a summation of emitted and reflected intensities.

The final discretized equation for a general control volume and control angle in three-dimensional geometry can be written as

$$a_P^{mn}I_P^{mn}=\sum_{I=\mathrm{E,W,N,S,T,B}} a_I^{mn}I_I^{mn}+b_P^{mn} \tag{6a}$$

where

$$a_I^{mn}=-\Delta A_i D_{\mathrm{ci,in}}^{mn} \tag{6b}$$

$$a_P^{mn}=\sum_{i=\mathrm{e,w,n,s,t,b}} \Delta A_i D_{\mathrm{ci,out}}^{mn}+\beta_{o,P}\Delta V\Delta\Omega^{mn} \tag{6c}$$

$$b_{\mathrm{P}}^{mn} = (\beta_{\mathrm{o}} S_{\mathrm{R}}^{mn})_{\mathrm{P}} \Delta V \Delta\Omega^{mn} \tag{6d}$$

$$S_{\mathrm{R}}^{mn} = (1-\omega_{\mathrm{o}}) I_{\mathrm{b}} + \frac{\omega_{\mathrm{o}}}{4\pi} \int_{\Omega'=4\pi} I^{m'n'} \Phi_{m'n'\to mn}\, \mathrm{d}\Omega' \tag{6e}$$

$$D_{\mathrm{ci}}^{mn} = \int_{\phi^{n-}}^{\phi^{n+}} \int_{\theta^{m-}}^{\theta^{m+}} (\vec{s}\cdot\vec{n}_i)\mathrm{d}\Omega \tag{6f}$$

$$D_{\mathrm{ci,in}}^{mn} = \int_{\Delta\Omega^{mn}} (\vec{s}\cdot\vec{n}_i)\mathrm{d}\Omega \qquad \vec{s}\cdot\vec{n}_i < 0 \tag{6g}$$

$$D_{\mathrm{ci,out}}^{mn} = \int_{\Delta\Omega^{mn}} (\vec{s}\cdot\vec{n}_i)\mathrm{d}\Omega \qquad \vec{s}\cdot\vec{n}_i > 0 \tag{6h}$$

where ΔA_i and $\vec{n}_i$ are the surface area and outward unit normal vector at the surface i, respectively. Here is adopted a step scheme in which a downstream face intensity is set to equal to the upstream nodal value. The discretization procedure and related quantities are easily found in Baek et al. [12].

In this study, the block-off method suggested by Chai et al. [14] is adopted to treat radiatively inactive regions such as slabs and dead zones. Fig. 2 shows a schematic of blocked-off regions. The point A is in a radiatively fully active cell, whereas D and S are in radiatively fully inactive cells. Although calculation is done over the whole domain, only solutions in the active region are meaningful. It must be noted that an additional source term is introduced into Eq. (6a) for block-off treatment as follows:

$$S^{\mathrm{A}} = S_{\mathrm{C}}^{\mathrm{A}} + S_{\mathrm{P}}^{\mathrm{A}} I_{\mathrm{P}}^{mn} \tag{7}$$

It becomes $S_{\mathrm{C}}^{\mathrm{A}} = 0$ and $S_{\mathrm{P}}^{\mathrm{A}} = -\mathrm{LN}$ (where LN is a large number) in inactive cells, whereas both $S_{\mathrm{C}}^{\mathrm{A}}$ and $S_{\mathrm{P}}^{\mathrm{A}}$ are equal to zero in active cells. The coefficients of Eqs. (6c) and (6d) are changed such that

$$a_{\mathrm{P}}^{mn} = \sum_{i=\mathrm{e,w,n,s,t,b}} \Delta A_i D_{\mathrm{ci,out}}^{mn} + \left(\beta_{\mathrm{o,P}} - S_{\mathrm{P}}^{\mathrm{A}}\right) \Delta V \Delta\Omega^{mn} \tag{8}$$

$$b_{\mathrm{P}}^{mn} = \left(\beta_{\mathrm{o}} S_{\mathrm{R}}^{mn} + S_{\mathrm{C}}^{\mathrm{A}}\right)_{\mathrm{P}} \Delta V \Delta\Omega^{mn} \tag{9}$$

The following conditions are imposed on an active cell, which is in direct contact with an inactive cell, as represented by point B in Fig. 2:

$$S_{\mathrm{C}}^{\mathrm{A}} = -\frac{\Delta A_{\mathrm{w}} D_{\mathrm{cw}}^{mn}}{\Delta V \Delta\Omega^{mn}} \left(\varepsilon_{\mathrm{w}} I_{\mathrm{b,w}} + \frac{1-\varepsilon_{\mathrm{w}}}{\pi} \sum I_{\mathrm{w}}^{m'n'} \left| D_{\mathrm{cw}}^{m'n'} \right| \Delta\Omega^{m'n'} \right) \tag{10}$$

$$S_{\mathrm{P}}^{\mathrm{A}} = 0 \tag{11}$$

where D_{cw}^{mn} is the directional weight at the bounding wall composed of $\vec{s}$ and $\vec{n}_{\mathrm{w}}$.

The whole domain is discretized into $(N_x \times N_y \times N_z)$ control volumes. Note that $\vec{n}_i$, ΔA_i and ΔV have to be calculated carefully according to grid skewness or curvature. Total solid angle, 4π steradians is divided into $(N_\theta \times N_\phi) = M$ directions, where θ is polar angle and ϕ is azimuthal angle, ranging from 0 to π and from 0 to 2π as shown in Fig. 1(b), respectively. Boundary condition in Eq. (5) for a diffusely emitting and reflecting wall can be discretized as

$$I_{\mathrm{w}}^{mn} = \varepsilon_{\mathrm{w}} I_{\mathrm{b,w}} + \frac{1-\varepsilon_{\mathrm{w}}}{\pi} \sum_{\vec{s}\cdot\vec{n}_{\mathrm{w}}<0} I_{\mathrm{w}}^{m'n'} \left| D_{\mathrm{cw,in}}^{m'n'} \right| \qquad \vec{s}\cdot\vec{n}_{\mathrm{w}} > 0 \tag{12}$$

Besides the wall boundary condition, intensity at symmetry planes is also required, for example, at $z = z_{\mathrm{s}}$ planes:

$$I(x,y,z_{\mathrm{s}},\theta,\phi) = I(x,y,z_{\mathrm{s}},\pi-\theta,\phi) \tag{13}$$

The iterative solution is terminated when the following convergence is attained:

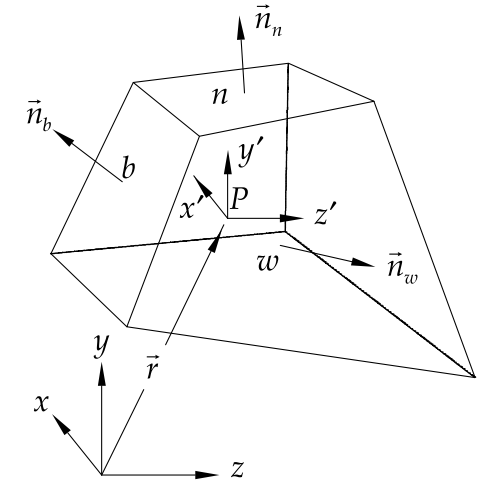

(a) control volume

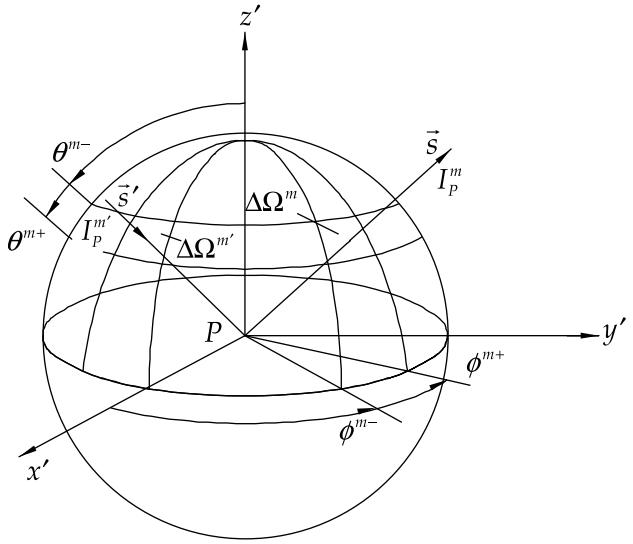

(b) control angle

Fig. 1. Schematics of control volume and control angle.

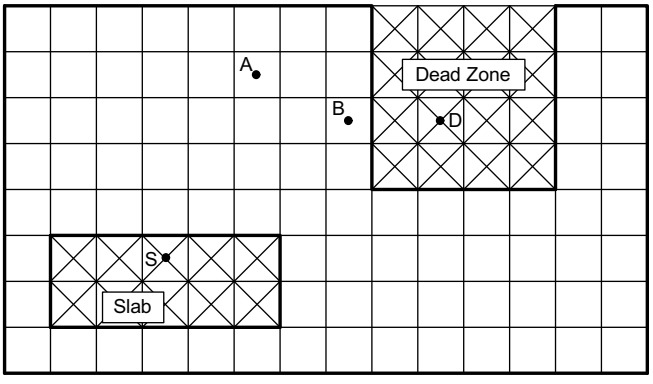

Fig. 2. Schematic of blocked-off regions.

$$\max\left[\left|I_{\mathrm{P}}^{mn} - I_{\mathrm{P}}^{mn,\mathrm{old}}\right| \Big/ I_{\mathrm{P}}^{mn}\right] < 10^{-6} \tag{14}$$

Here $I_{\mathrm{P}}^{mn,\mathrm{old}}$ is the previous iteration value of I_{P}^{mn}.

Once the intensity field is obtained, the radiative heat flux into wall including a slab surface can be estimated as follows:

$$q_{\mathrm{w}}^{\mathrm{R}} = \int_{\Omega=4\pi} I(\vec{r}_{\mathrm{w}}, \vec{s})(\vec{s}\cdot\vec{n}_{\mathrm{w}})\mathrm{d}\Omega = \sum I_{\mathrm{w}}^{mn} D_{\mathrm{cw}}^{mn} \tag{15}$$

2.3. Weighted sum of gray gas model (WSGGM)

Modest [15] has shown that the WSGGM can be used with any solution method after replacing the non-gray medium by an equivalent small number of gray medium with constant absorption coefficients:

$$I = \sum_k I_k \tag{16}$$

$$\frac{1}{\beta_{0,k}}\frac{\mathrm{d}I_k}{\mathrm{d}s} = -I_k + (1-\omega_{0,k})f_{\varepsilon,k}I_{\mathrm{b}} + \frac{\omega_{0,k}}{4\pi}\int_{\Omega'=4\pi} I_k(\vec{s}')\Phi(\vec{s}'\to\vec{s})\mathrm{d}\Omega' \tag{17}$$

$$f_{\varepsilon,k} = 1 - \sum_{j=1}^{J} b_{\varepsilon,k,j}T^{j-1} \tag{18}$$

where $b_{\varepsilon,k,j}$ are referred to as the emissivity gas temperature polynomial coefficients as found in Smith et al. [16]. The total intensity I can be found by just summing up all the kth gray gas intensities. Eq. (17) is the radiative transfer equation for the kth gray gas with constant absorption coefficient, with blackbody intensity I_{b} replaced by a weighted intensity $f_{\varepsilon,k}I_{\mathrm{b}}$. This weighted sum of gray gases model takes account of radiative effects by non-gray gases such as CO_2 and H_2O in gas mixture. More detailed descriptions of WSGGM are easily found in Modest [15].

3. Results and discussion

3.1. Configuration of the furnace

The furnace is very big in its scale and there exist lots of slabs inside the furnace, so it is inevitable to use large size of grid. Moreover, a slab should have appropriate grid spacing, otherwise the solution changes with grid. It is necessary to take relevant grid spacing for a slab. In addition to geometrical grid, solid angle is also discretized, so actual computational array size is increased as much as multiplied by discretization number of solid angle. This is why the radiation code developed here was parallelized to be run on clustered PCs by using MPI library. The parallelization makes it possible to overcome deficiency of physical memory as well as to save computing time.

Fig. 3 shows the half section of the reheating furnace. The furnace is symmetric along the $y = 0$ plane, so calculation is performed on the half section of the furnace. The coordinates system is set to increase the performance of parallelization. The furnace has the dimension of 5.4 m × 10.7 m × 36.0 m. A furnace is divided into three zones – preheating, heating, and soaking zones. Slabs are mostly heated in the preheating and heating zone. The role of soaking zone is to reduce the slabs' temperature distribution in the slabs. Twenty-nine slabs are heating in the furnace and they experience about 2 h heating. The slabs have the dimension of 0.23 m × 4.8 m × 1.0 m and they are located at the elevation of 0.21 m from the furnace bottom.

3.2. Simulation of the furnace

The entire computational domain is divided into eight subzones to specify temperature distribution as shown in Fig. 4. Usually upper region – above slabs – has higher temperature than lower region. Vertically, the entire domain is divided into two sections with respect to slabs. Horizontally, it is divided into four sections. Horizontal four sections are formed by spliting preheating zone into two sections, while the other two zones remain unsplited. Each sub-zone has constant wall and gas temperatures as shown in Table 1. The gas temperature is set to the value which is 200 K higher than the wall temperature. The composition of gas is set to be uniform throughout the entire sub-zones – H_2O: 0.173, CO_2: 0.113, O_2: 0.015, N_2: 0.699 in mass fraction.

Fig. 5 shows the computational grid of the furnace. The size of grid is 67 × 70 × 415 and 1,946,350 cells are formed. Slabs have the grid size of 8 × 48 × 14. Grid is clustered inside the slabs along the thickness direction. N_θ and N_ϕ – solid angle split number – have the value of 4 and 12, respectively. Slabs move every 256 s and

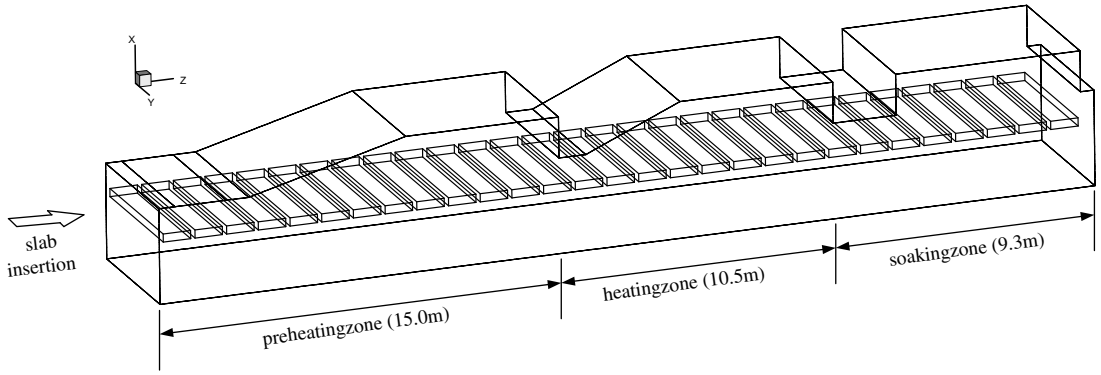

Fig. 3. Shape of the furnace.

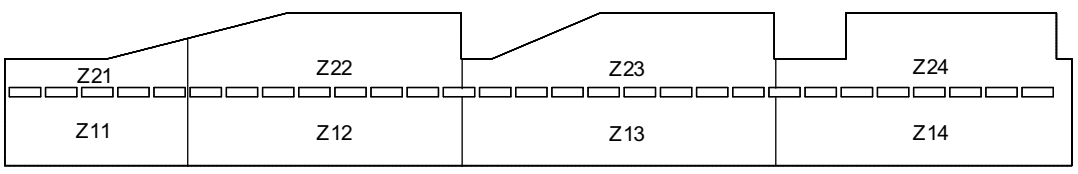

Fig. 4. Sub-zones of the entire domain.

Table 1
Temperature distribution of eight sub-zones (K)

		Preheating zone		Heating zone	Soaking zone
		Former	Later		
Upper	Wall	1023	1273	1323	1233
	Gas	1223	1473	1523	1433
Lower	Wall	973	1223	1253	1143
	Gas	1173	1423	1453	1343

Table 2
Properties of slab

Temperature (K)	Conductivity (W/m K)	Specific heat (J/kg K)	Emissivity
$T < 473$	60.57	504.0	0.5
$473 < T < 673$	51.17	577.9	0.5
$673 < T < 873$	41.74	712.3	0.5
$873 < T < 1073$	34.04	892.1	0.5
$1073 < T < 1273$	28.08	730.8	0.6
$1273 < T$	29.81	672.0	0.6

they reside in the furnace for 7424 s. Total computational time is equal to slab residence time and the physical time step for calculation is 32 s. Computation is performed on a 16 clustered PCs (3 GHz CPU). The emissivity of furnace walls is set to be 0.75. The density of slab is 7854 kg/m^3 while the other properties of slab are listed in Table 2. Slabs are introduced into the furnace at 293 K, i.e., clod charging of slabs.

Fig. 6 depicts radiation flux vector on $J = 40$ slice. Radiation emitted by hot gas impinges on the furnace wall and the slabs. Temperature difference is a potential for driving radiation flux. So large radiation flux is produced between hot gas and slabs and large heat flux vector is formed around the slabs. Because the temperature difference between slabs and hot gas is bigger than that of between the furnace walls and hot gas, most of the radiation flux from hot gas flows into the slabs. Fig. 7 shows three integrated incident radiation fluxes into the slabs – on all the surfaces, on the top surface, and on the bottom surface of each slab. The slabs in the preheating and heating zones receive large portion of radiation flux. Among the slabs, eighth slab receives largest radiation flux. Radiation flux becomes weak in soaking zone. It is because slabs already have experienced enough heating in previous zones and the temperature difference becomes very small. Moreover, radiation flux is coming out from bottom of the slabs in the soaking zone.

When a slab is heated up, its corners are heated faster than any other region. Three surfaces adjoin on each corner of the slab, where heat penetrates into the slab in three directions. This is compared to the only one direction into the plain surface region. Fig. 8 confirms this phenomenon. Highest temperature spots are located on the corners of the slab and lower temperature zones are formed in the inner area of all the surfaces. Large temperature difference inside a slab is mainly caused by this fast heating of corners. Another main cause of temperature distribution is a skid system but it is not considered in this study. Skid system keeps temperature low in the contact area between a slab and a skid system by shielding radiation flux.

Fig. 9 shows the volume averaged temperature, the area averaged temperature on the bottom and top surfaces, and maximum temperature difference inside a slab. The slabs are emitted to rolling mill at about 1273 K. In the soaking zone, slabs stay at almost same temperature but the temperature difference continuously decreases until a slab reaches 26th position. From the 26th position, the decreasing rate of temperature difference reduces to small quantity. Top surface temperature always stays higher than the bottom surface temperature. But a reversion occurs between bottom surface and volume mean temperatures at 22nd slab. Since then, lowest temperature is located on the bottom surface and conductive heat flux directs downward, while conductive heat flux directs inward before then. Mean temperature of a slab should stay at target temperature and temperature difference should stay below 50 K/m. This requirement is satisfied from 26th slab.

3.3. Variation of residence time

Calculation is performed to investigate the appropriateness of the heating time. Three more cases of residence time – 5670, 6496, and 6960 s are tried for the inspection. In previous section, a slab satisfies the requirement from 26th position, so there is a possibility to increase the performance. Target temperature is to be 1273 K because slab temperature converges to it under the given furnace wall and gas temperature. It is turned out that the residence times of 5568 and 6496 s are not appropriate. Fig. 10 shows that temperature difference remains over 50 K all the heating time for the cases of 5568 and 6496 s. The case of 6960 s satisfies the temperature difference requirement from the 28th slab and reaches close to the target temperature.

Further a slab moves into the hot gas field, the higher the radiation flux to the slab grows. Fig. 11 shows that the radiation flux increases after insertion. But radiation flux does not continue to increase because the temperature rise of a slab derives the radiation flux to decrease. So there exists a location at which maximum radiation flux occurs. It occurs at the ninth slab for the residence times of 5568 and 6496 s. The cases of 6960 and 7424 s have the maximum at the eighth slab. The radiation flux turns to decreases right after reaching maximum due to rapid temperature rise of slabs in case of 7424 s. But relatively wide peak is formed in case of 5568 s. The result shows that the increased potential by slab's further entrance into hot gas field enough compensates for the temperature rise of a slab for the case of 5568 s. The radiation fluxes of all the cases are almost equal to each other before reaching their maximum value. This means that the temperature of a slab is not a deterministic factor of the radiation flux in the initial stage of heating for cold charging of slabs.

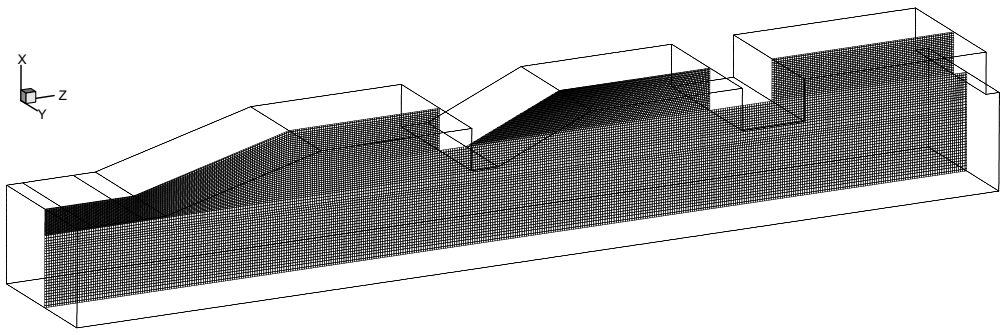

Fig. 5. Computational grid.

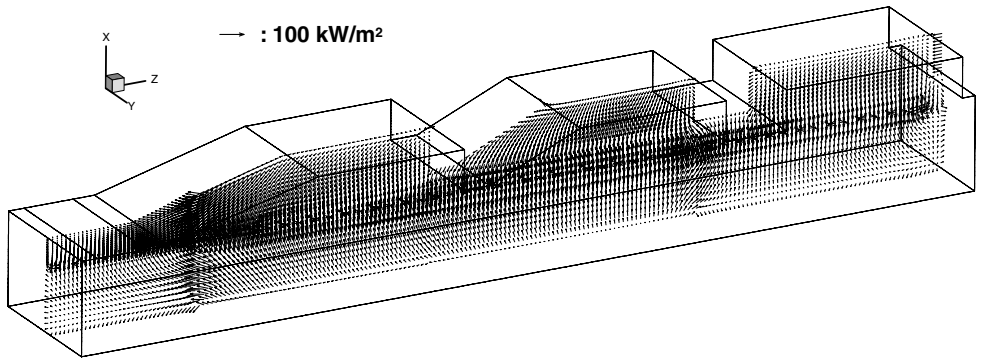

Fig. 6. Radiation flux vector on $J = 40$ slice.

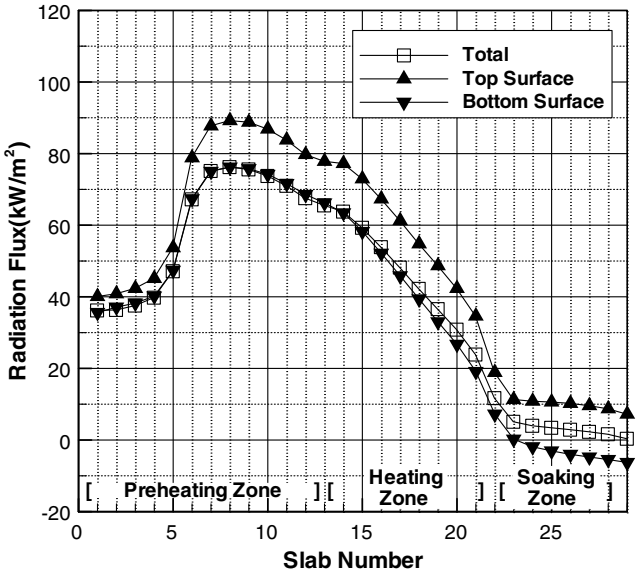

Fig. 7. Radiation fluxes into the slabs.

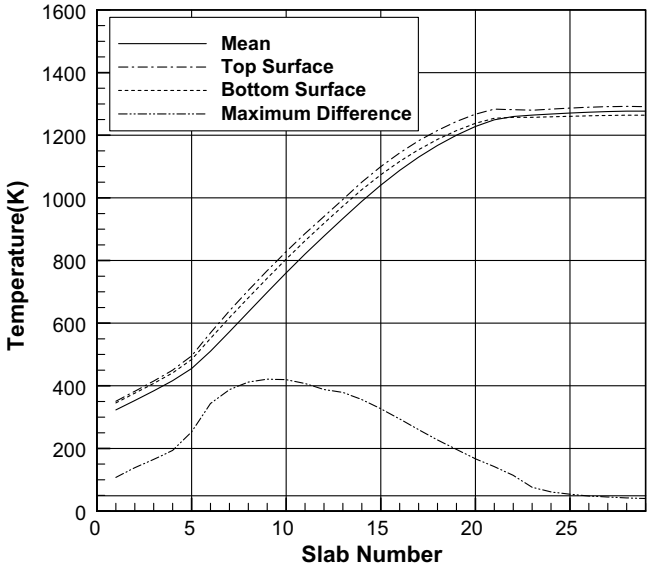

Fig. 9. Various temperature profiles.

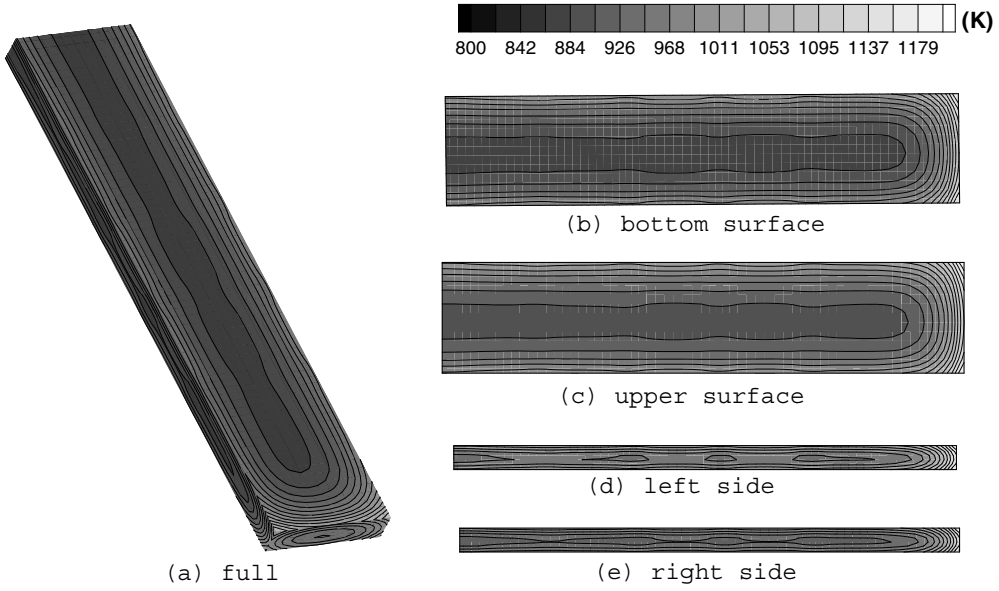

Fig. 8. Temperature contour of the 10th slab.

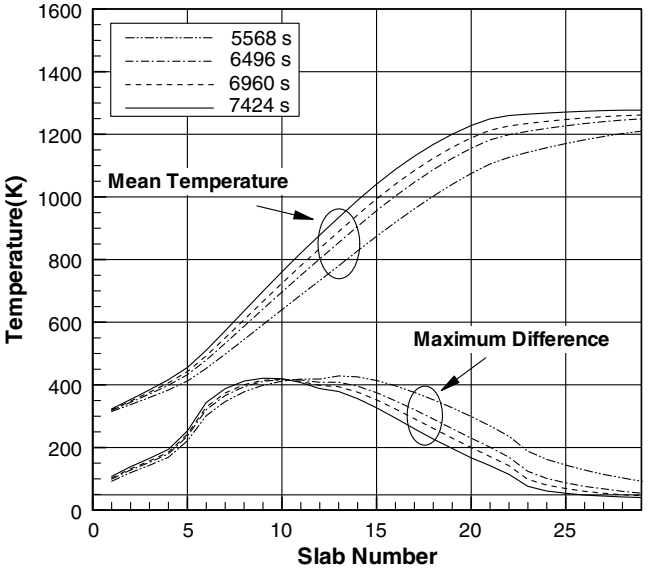

Fig. 10. Temperature profiles for the various residence times.

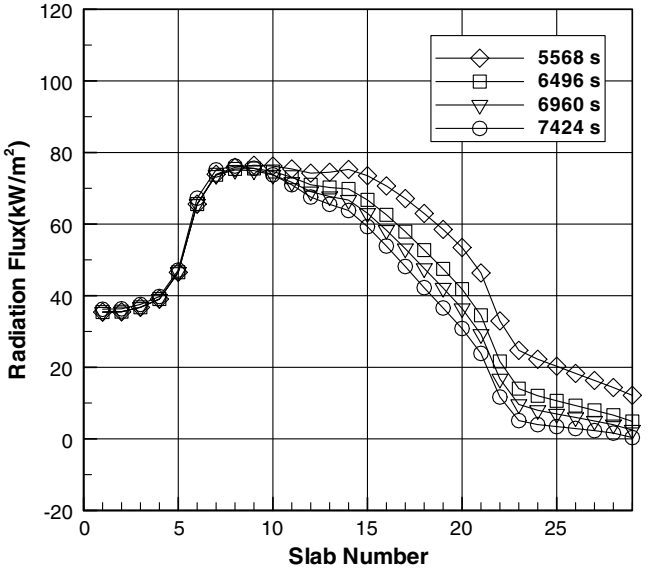

Fig. 11. Radiation fluxes for the various residence times.

4. Conclusion

A numerical simulation was performed to investigate the radiative heating characteristics of the slabs in a reheating furnace of POSCO incorporation. The radiation flux to each slab inside the furnace is calculated by using parallelized FVM radiation code and it is used for the boundary condition of the heat conduction equation governing slab temperature. Precise observation of heating characteristics was carried for the given slab residence time and the effects of slab residence time on heating slabs were investigated.

It is observed that most radiation flux occurs at preheating zone and heating zone. In soaking zone, slabs receive little radiation flux from the environment, so slab temperature is hardly raised but degree of temperature uniformity is further developed. The eighth slab receives largest radiation flux for the given residence time (7424 s).

Of the four cases of residence time, the residence times of 6960 and 7424 s satisfy the temperature uniformity requirement. The temperature uniformity requirement is satisfied from the 26th slab in case of 7424 s and from the 28th slab in case of 6960 s. Their emission temperatures reach close to the target temperature of 1273 K.

Acknowledgements

This work was supported by the Combustion Engineering Research Center at the Department of Mechanical Engineering, Korea Advanced Institute of Science and Technology, which is founded by the Korea Science and Engineering Foundation.

References

[1] R. Ford, N.V. Suryanarayana, J.H. Johnson, Heat transfer model for solid-slab/water-cooled skid pipe in reheat furnace, Ironmak. Steelmak. 7 (1980) 140–146.
[2] S.H. Han, S.W. Baek, S.H. Kang, C.Y. Kim, Numerical analysis of heating characteristics of a slab in a bench scale reheating furnace, Int. J. Heat Mass Transfer 50 (2007) 2019–2023.
[3] Zongyu Li, P.V. Barr, J.K. Brimacombe, Computer simulation of the slab reheating furnace, Can. Metall. Quart. 27 (1988) 187–196.
[4] A. Jaklic, T. Kolenko, B. Zupancic, The influence of the space between the billets on the productivity of a continuous walking-beam furnace, Appl. Therm. Eng. 25 (2005) 783–795.
[5] M.F. Modest, Radiative Heat Transfer, McGraw-Hill, New York, 1993.
[6] B.G. Carlson, K.D. Lathrop, Transport Theory – The Method of Discrete Ordinated in Computing Methods in Reactor Physics, Gordon & Breach Science Publishers, New York, 1968.
[7] W.A. Fiveland, Discrete ordinates solutions of transport equation for rectangular enclosure, ASME J. Heat Transfer 106 (1984) 699–706.
[8] E.H. Chui, G.D. Raithby, Computation of radiant heat transfer on a nonorthogonal mesh using the finite-volume method, Numer. Heat Transfer B 23 (1993) 269–288.
[9] J.C. Chai, H.S. Lee, S.V. Patankar, Finite volume method for radiation heat transfer, J. Thermophys. Heat Transfer 8 (1994) 419–425.
[10] J.C. Chai, A Finite-Volume Method for Radiation Heat Transfer, Ph.D. Thesis, University of Minnesota, Minneapolis, MN, 1994.
[11] M.Y. Kim, S.W. Baek, Numerical analysis of conduction, convection, and radiation in a gradually expanding channel, Numer. Heat Transfer A 29 (1996) 725–740.
[12] S.W. Baek, M.Y. Kim, J.S. Kim, Nonorthogonal finite-volume solutions of radiative heat transfer in a three-dimensional enclosure, Numer. Heat Transfer B 34 (1998) 419–437.
[13] J.Y. Murthy, S.R. Mathur, Finite volume method for radiative heat transfer using unstructured meshes, J. Thermophys. Heat Transfer 12 (1998) 313–321.
[14] J.C. Chai, H.S. Lee, S.V. Patankar, Treatment of irregular geometries using a Cartesian coordinates finite-volume radiation heat transfer procedure, Numer. Heat Transfer B 26 (1994) 225–235.
[15] M.F. Modest, The weighted-sum-of-gray-gases model for arbitrary solution methods in radiative transfer, ASME J. Heat Transfer 113 (1991) 650–656.
[16] T.F. Smith, Z.F. Shen, J.N. Friedman, Evaluation of coefficients for the weighted sum of gray gases model, ASME J. Heat Transfer 104 (1982) 602–608.